ceramics

MDPI

Article

Increasing the Flow Stress during High-Temperature Deformation of Aluminum Matrix Composites Reinforced with TiC-Coated CNTs

Artemiy V. Aborkin *, Dmitriy V. Bokaryov, Sergey A. Pankratov and Alexey I. Elkin

Department of Mechanical Engineering Technology, Vladimir State University Named after Alexander and Nikolay Stoletovs, 600000 Vladimir, Russia
* Correspondence: aborkin@vlsu.ru

Abstract: In this work, composites based on AA5049 aluminium alloy reinforced with multiwalled carbon nanotubes (CNTs) and multiwalled TiC-coated CNTs were prepared by powder metallurgy. For the first time, the effect of TiC coating on the CNT surface on the flow stress of aluminum matrix composites under compressive conditions at 300–500 °C has been investigated. It was found that composites reinforced with TiC-coated CNTs have a higher flow stress during high-temperature deformation compared to composites reinforced with uncoated CNTs. Moreover, with an increasing temperature in the 300–500 °C range, the strengthening effect increases from 14% to 37%. Compared to the reference sample of the matrix material without reinforcing particles, obtained by the same technological route, the composites reinforced with CNTs and CNT-hybrid structures had a 1.8–2.9 times higher flow stress during high-temperature deformation. The presented results show that the modification of the CNTs surface with ceramic nanoparticles is a promising structure design strategy that improves the heat resistance of aluminum matrix composites. This extends the potential range of application of aluminum matrix composites as a structural material for operation at elevated temperatures.

Keywords: carbon nanotubes; TiC coating; hot deformation; aluminum matrix composite; compression; properties; flow stress

Citation: Aborkin, A.V.; Bokaryov, D.V.; Pankratov, S.A.; Elkin, A.I. Increasing the Flow Stress during High-Temperature Deformation of Aluminum Matrix Composites Reinforced with TiC-Coated CNTs. *Ceramics* **2023**, *6*, 231–240. https://doi.org/10.3390/ceramics6010013

Academic Editors: Amirhossein Pakseresht and Kamalan Kirubaharan Amirtharaj Mosas

Received: 27 November 2022
Revised: 23 December 2022
Accepted: 5 January 2023
Published: 10 January 2023

1. Introduction

The modern industry needs lightweight yet tenacious materials. Aluminum alloys have met these requirements for many years. However, despite the economic availability of these materials, the limiting factor for their use is often their low strength at elevated temperatures. Typically, the operating temperature limit for aluminum alloys does not exceed 200–300 °C [1]. It is possible to increase the operating temperature range of aluminum alloys by creating particulate-reinforced composites on their basis by controlling the properties by selecting the type, size and shape of reinforcing particles. Liquid-phase or solid-phase methods [2–4] for creating bulk composites, as well as various methods of depositing coatings and surface modification [5–10], can be used for this purpose. Great progress in this direction has been achieved in the production of so-called sintered aluminum powders (SAP's) [1,11–14], which are, in fact aluminum matrix composites reinforced with Al_2O_3 particles. These materials exhibit relatively high strength properties even at ~0.85 Tm of the matrix alloy. For example, in the study [1], the in situ formation of an Al_2O_3 shell on an aluminum surface provided the preservation of the strength of a material in the range of 140 to 120 MPa at 0.66–0.88 Tm (350–520 °C). In [14], it was shown that the addition of 1.5 wt.% Al_2O_3 facilitates the measurement of the compression strength of the Al7075 alloy at the level of 260–125 MPa at 0.61–0.82 Tm (300–500 °C).

One of the promising types of reinforcing particles, due to their unique physical and mechanical properties, are carbon nanotubes (CNTs). The Young moduli of CNTs,

depending on their chirality, number of walls, diameter and defectiveness of their structure, can reach from ~1 to 4 TPa [15–19], and the axial tensile strength is 63–110 GPa [18,19]. Despite this, the effective utilization of the load-bearing potential of CNTs in aluminum matrix composites at high temperature is hindered by their tendency to react chemically with the matrix aluminum alloy. This leads to the in situ formation of the Al_4C_3 phase, compromising the structural integrity of CNTs. For example, in [20], it was shown for the 2009 Al alloy composite reinforced with 1.5 vol.% CNTs that, after increasing temperature from 20 to 300 °C, the yield strength increment decreases from ~100 to ~30 MPa, and in the case of 4.5 vol.% CNTs, a decrease in the yield strength of the composite material at 300 °C was noted even in comparison with the matrix material without reinforcement. It should be noted that this is also characteristic of aluminum matrix composites reinforced with carbon microfibers. For instance, paper [21] reports that AA7075 alloy reinforced with 15 vol.% carbon fibers with an average diameter of 10 μm shows a 5-fold decrease in compressive flow stress from 750 MPa to 150 MPa at an increasing temperature from 25 °C to 300 °C. A more recent work [22] shows an increase in the strengthening effect when the CNTs volume fraction increases from 2.5 to 5 vol.%, which can be explained by a rather homogeneous distribution of nanotubes in the aluminum matrix. At the same time, the strengthening effect at 200 °C was greater than at 400 °C. The authors attributed this to the higher recrystallization resistance of the composite compared to the matrix material. The reduction of the strengthening effect with increasing test temperature from 200 °C to 400 °C is attributed to the fact that, at this temperature, the CNTs could no longer so effectively prevent grain boundary movement.

Considering the above, it seems promising to use CNT-hybrid nanostructures with ex situ modified CNTs as reinforcing additives. Such a modified surface of CNTs will contribute to the formation of an interfacial layer at the Al–CNT interface [23–28]. The presence of an ex situ interfacial layer, for example, TiC carbide ceramics, on the surface of CNTs should improve the interfacial interaction by increasing adhesion [29,30] and also prevent unwanted chemical reactions with the matrix leading to the structural degradation of CNTs [31].

The purpose of this work is to investigate the effect of TiC coating on the surface of CNTs on increasing the flow stress at high temperature of aluminum matrix composites.

2. Materials and Methods

The initial multiwall CNTs were synthesized by the MOCVD method with ferrocene and toluene used as precursors under argon flow in a tubular reactor equipped with a tubular furnace at 825 °C, as described in detail elsewhere [32]. The deposition of titanium carbide nanoparticles on the surface of CNTs was performed by the thermal decomposition of titanocene dichloride vapors according to the procedure described in detail earlier [33].

The initial matrix material was in the state of granules of aluminum alloy AA5049 1–2 mm in size. The elemental composition of the granules measured using an ARL ADVANT'X (Thermo Scientific) sequential X-ray fluorescence spectrometer was as follows (wt.%): Al 96.11; Mg 2.42; Mn 0.55; Fe 0.26; Si 0.37; Zn up to 0.1; Ti up to 0.1; Cu to 0.1.

Granules of aluminum alloy with reinforcing additives (named as CNT or TiC/CNT for simplicity hereafter) were mixed by high-energy ball milling (HEBM) using a PULVERISETTE 6 planetary mill (Fritsch, Idar-Oberstein, Germany). For this purpose, aluminum alloy granules, reinforcing particles (CNT or TiC/CNT, 1 wt.%), and a process control agent (stearic acid, 0.8 wt.%) were placed in a 250 mL stainless steel vessel in which grinding balls of hardened steel 100 × 6 with a diameter of 8 mm were also added. The ball-to-powder weight ratio was 15:1. The processing speed and time were 600 rpm and 6 h, respectively. Thus, composite powders named A_CNT or A_TiC/CNT for simplicity hereafter and a reference sample of matrix alloy powder without reinforcing particles named A_m were obtained. The milled composite powders were hot-pressed in a special heated steel die at 450 °C and 350 MPa to obtain compacts with a diameter of 17 mm and a height

of 12 mm. The consolidation modes were adopted, considering the recommendations of [34].

The surface morphology of the initial CNTs, TiC-coated CNTs and synthesized composite powders were studied using a Zeiss 55 Ultra scanning electron microscope (Carl Zeiss AG, Jena, Germany). The particle size analysis of the powders was carried out with a Microsizer 201C laser analyzer (Moscow, Russia).

The phase composition of CNTs, CNT-hybrid structures, composite powders and bulk samples was studied with the XRD method using a D8 ADVANCE (BRUKER, Bremen, Germany) with Cu Kα radiation (λ = 1.5148 Å, 40 kV and 40 mA) and linear detection at angles of 25–85°. The crystallite size was calculated from XRD data using the Scherer relation for the main diffraction peak of aluminum (111). The instrumental broadening was determined using a standard α-Al_2O_3 sample.

The bulk samples were investigated by Raman spectroscopy Integra Spectra (NT-MDT, Moscow, Russia) at 473 nm with no more than 50 mW. The Raman spectra were measured at more than 10 different points on each sample.

The surface porosity was determined on metallographic sections using an Altami Met 1-C optical microscope (Moscow, Russia). The quantitative analysis of surface porosity was performed using ImageJ software. At least 10 images were studied (the surface area was ~3.5 mm^2).

Compression tests at elevated temperatures were performed on a universal testing machine WDW-100E (Time Group Inc., Beijing, China) in a special thermal cell at temperatures of 300, 400 and 500 °C and a compression rate of 0.1 s^{-1}. Cylindrical samples for compression testing at elevated temperatures with a diameter of 6 mm and a height of 12 mm were obtained by electroerosive cutting on a Mitsubishi BA8 machine. Graphite was used to reduce friction on the end surfaces of the specimens. The choice of the lower boundary of the test temperature interval corresponds to the limiting operating temperature of aluminum alloys. The upper boundary of the range is the limit in most of the published investigations. The compression rate was taken for the possibility of comparing the data of this work with those published in other sources as one of the most frequently used.

The results of calculating the volume fraction of reinforcing nanostructures using the model given in [27] show that the volume fraction of the reinforcement in CNT-reinforced composite was 1.2 vol.%, and in TiC/CNT-reinforced composites, it was 0.65 vol.%.

3. Results and Discussion

The results of the characterization of the structural-phase composition of reinforcing nanoparticles of both types used in this study using scanning electron microscopy and X-ray diffractometry are shown in Figure 1.

The SEM images show that the initial CNTs have a diameter of ~60–100 nm and a length of a few micrometers (see Figure 1a). After TiC coating, the CNTs diameter increases to ~160–180 nm (see Figure 1b). The carbide coating on the CNTs' surface has a relatively smooth and continuous morphology. Figure 1b,d shows the XRD results of initial CNT and TiC/CNT. The initial CNTs are characterized by the presence of (002), (100), (101), and (004) carbon lines. The TiC/CNT structures contain, similarly to the original CNT, a carbon phase and fcc-TiC, for which (111), (200), (220), and (311) peaks are clearly recorded. Thus, the data presented show that, during MOCVD treatment, a TiC coating is formed on the surface of the initial CNT.

Typical SEM images of the morphology of powders obtained by the HEBM method are shown in Figure 2. The synthesized powders are characterized by a rounded shape. The average particle size was 50–60 μm. The results of the particle size analysis of the synthesized powders are shown in Figure 2d. Combined analysis of the SEM images and particle size data shows that the reinforcing particles contribute to a slightly more intense refinement of the matrix alloy particles. For example, the average particle size of the matrix powder without reinforcing particles was 60.5 μm. The particle size of composite powder reinforced with 1 wt.% CNT and TiC/CNT was 51.3 and 54.8 μm, respectively. Therefore,

it can be concluded that the average particle size of the composite powder decreases with the increasing volume fraction of reinforcing nanostructures.

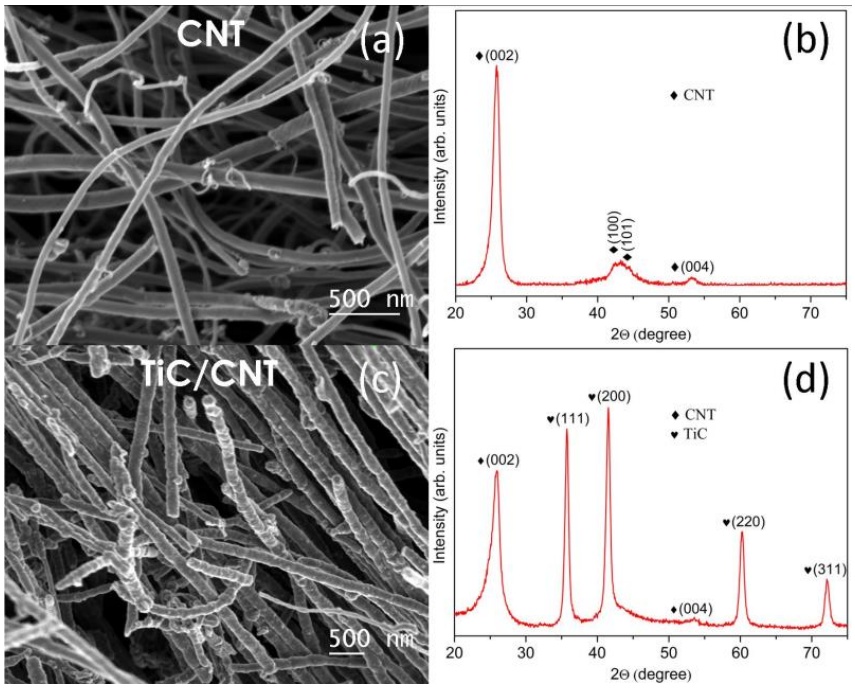

Figure 1. SEM image of pristine CNTs (**a**), TiC/CNT (**b**), XRD of pristine CNTs (**c**), TiC/CNT (**d**).

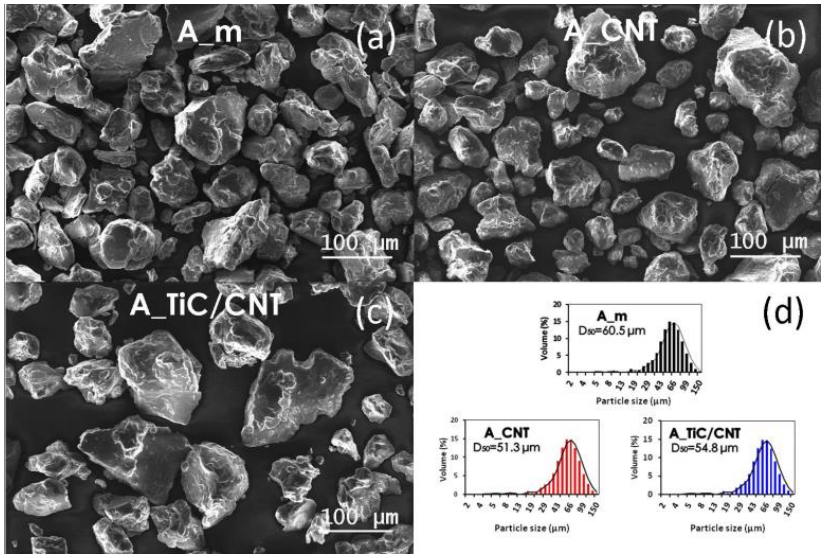

Figure 2. SEM images of matrix alloy powders after HEBM (**a**), CNT-reinforced composite (**b**) and TiC/CNT-reinforced composite (**c**), and particle size analysis of these powders (**d**).

The XRD results of the powder materials and bulk samples are shown in Figure 3. The data obtained for the powder and bulk samples are qualitatively similar. They clearly show (111), (200), (220), (311) and (222) aluminum peaks. At the same time, no diffraction peaks of the reinforcing phases were observed. In general, this is typical for aluminum alloys reinforced with carbon nanostructures even at higher concentrations of reinforcing additives.

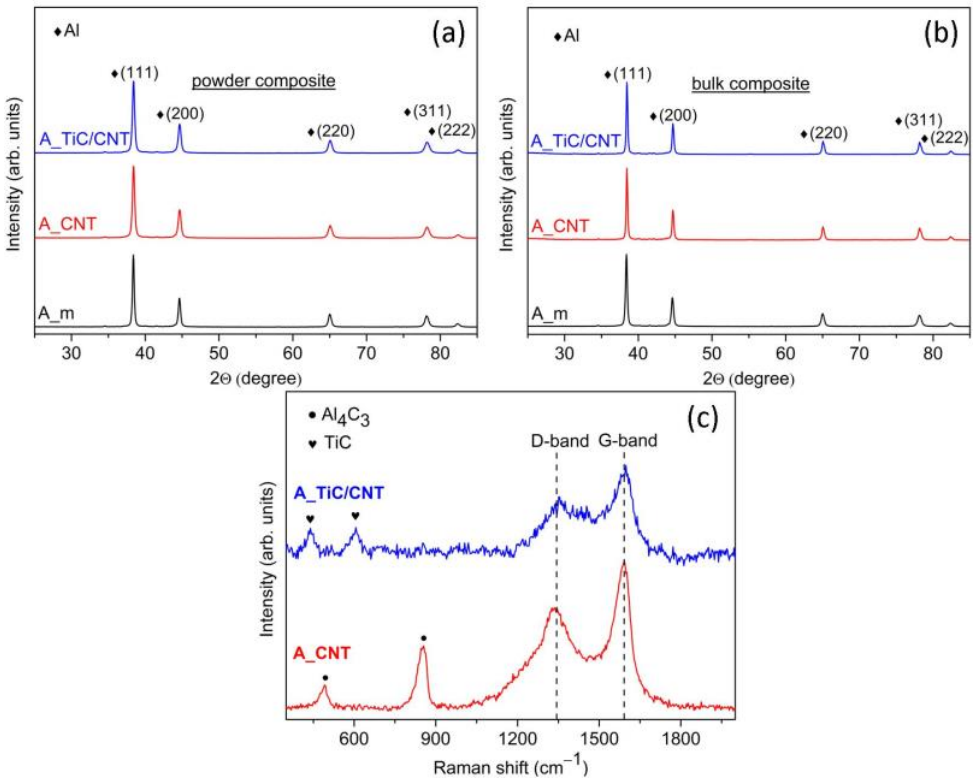

Figure 3. XRD data of powder materials (**a**), bulk samples (**b**) and Raman spectroscopy results of bulk samples (**c**).

In addition, it can be noted that the FWHM for bulk samples decreases compared to powder samples. This indicates an increase in crystallite size during isothermal holding during consolidation. For composite samples A_CNT and A_TiC/CNT containing reinforcing nanostructures, a smaller increase of crystallite size was observed in comparison to A_m without reinforcing additives. This may indicate the anchoring of grain boundaries in the composite materials due to reinforcing nanoparticles. Moreover, A_TiC/CNT samples are characterized by a smaller crystallite size both after ball milling and after consolidation, as compared to A_CNT samples. This may be due to the better distribution of CNT-hybrid nanostructures during ball milling because of their lower volume fraction. Since the XRD data do not contain information on the reinforcing particles and ceramic coating, the Raman spectroscopy of bulk samples was performed (see Figure 3c). The Raman spectroscopy of bulk A_TiC/CNT composites shows the presence of D- and G-lines at ~1350 cm^{-1} and ~1600 cm^{-1} belonging to CNT. In addition, lines at 439 cm^{-1} and 606 cm^{-1} belonging to the TiC-coating are identified. At the same time, the Al_4C_3 lines are absent. At the same time, the Al_4C_3 lines at ~490 cm^{-1} and ~855 cm^{-1} are clearly detected for the A_CNT composites in addition to the D- and G-lines. This shows that the presence of the TiC coating on the CNT surface prevents the formation of in situ Al_4C_3 and acts as a barrier interphase layer between the matrix alloy and CNT.

Figure 4 shows the optical microscopy microstructure of the bulk samples and the surface porosity data. A comparative analysis of the microimages shows that all the bulk samples have low residual porosity (see Figure 4d). This could be an indication that the consolidation mode was chosen correctly.

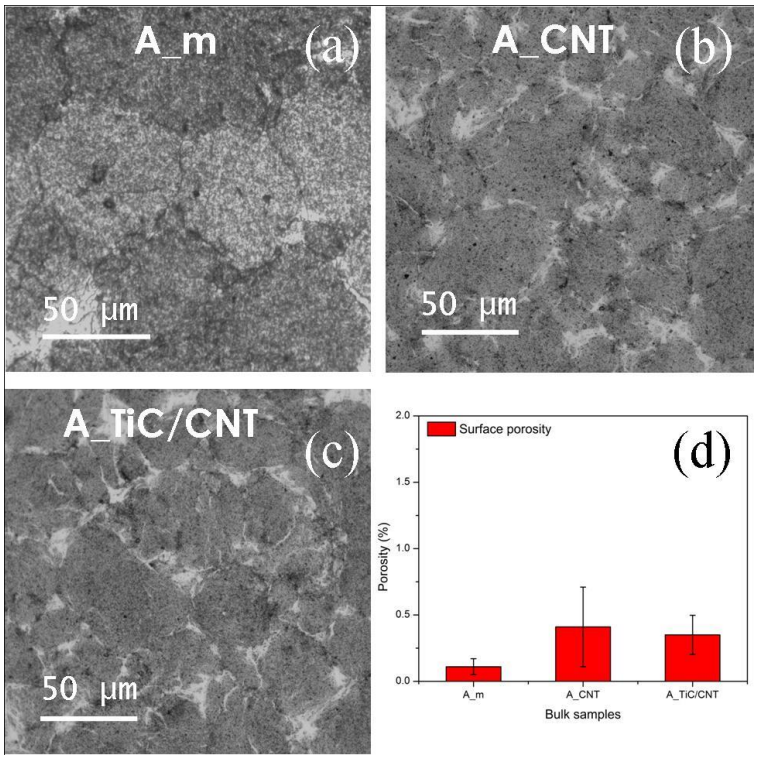

Figure 4. Optical images of the microstructure of bulk samples of matrix material (**a**), CNT-reinforced composite (**b**), TiC/CNT-reinforced composite (**c**) and surface porosity data of these samples (**d**).

Figure 5 shows the engineering curves for compression tests on bulk specimens at 300–500 °C. The flow stress curves are characterized by the presence of sections corresponding to the processes of the strengthening and softening in the deformed material. At 300–400 °C for all the materials tested at the initial stage, the strengthening processes are dominant, which is expressed in the presence of a "hill". This is due to the necessity of energy accumulation for the realization of thermally activated softening mechanisms. In this case, at 500 °C, strengthening and softening processes are balanced. This is due to the higher mobility of the boundaries at this temperature, which contributes to more intensive nucleation and growth of dynamically recrystallized grains as well as more intensive destruction of dislocations. The increased flow stress of composites as compared to the reference matrix material sample is explained, on the one hand, by the inherent submicron structure formed at the HEBM stage and retained during consolidation and, on the other hand, by the presence of reinforcing nanoparticles on the matrix alloy grain boundaries, preventing both the dislocation motion and the boundaries themselves during recrystallization.

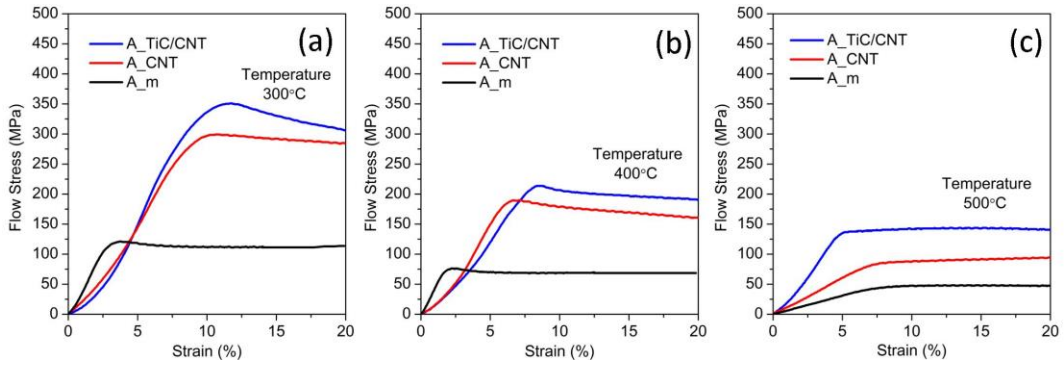

Figure 5. Compression flow stress curves at 300 °C (**a**), 400 °C (**b**), 500 °C (**c**) and strain rate 0.1 s^{-1}.

As expected, an increase in temperature led to a decrease in the flow stress of the bulk samples. For example, an increase in temperature from 300 to 500 °C resulted in a decrease of flow stress from 300 to 86 MPa and from 350 to 137 MPa for A_CNT and A_TiC/CNT, respectively. This clearly demonstrates the positive effect of TiC coating on the CNTs surface on the increase of flow stress during the high-temperature deformation of aluminum matrix composites. Besides, composites reinforced with both TiC/CNT and CNT showed greater flow stress during high-temperature deformation compared to the reference sample A_m of the matrix material obtained by the same process route. Thus, CNT-reinforced composites have on average 1.8–2.5 times higher flow stress at the specified temperatures compared to A_m. Moreover, with increasing temperature, the strengthening effect for A_m CNT decreased. This is consistent with the data reported in [22]. In contrast, the strengthening effect for A_TiC/CNT was constant over the temperature range in question and the TiC/CNT-reinforced composites had 2.9 times higher flow stress than the A_m reference sample. This is due to the fact that in situ Al_4C_3 formation occurs in CNT-reinforced composites, which compromises the structural integrity of CNTs and reduces their bearing capacity. The TiC barrier coating inhibits this reaction, which leads to a more efficient use of the CNT's load-bearing potential. Considering this, it can be assumed that A_TiC/CNT can also operate at temperatures higher than 500 °C. However, this requires further investigations.

To correlate the obtained results with the published data on aluminum alloys and aluminum matrix composites reinforced with other types of micro- and nanoparticles, summary graphs (see Figure 6) of the change in flow stress depending on temperature at a deformation rate of 0.1 s^{-1} are presented.

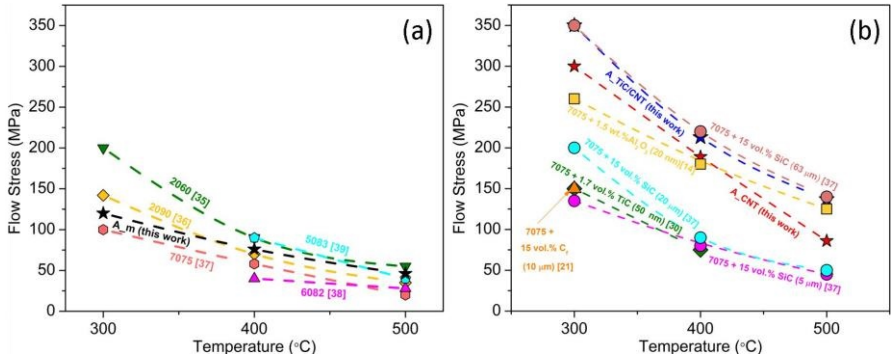

Figure 6. Flow stress of aluminum alloys (**a**) and composites based on them (**b**) at temperature 300–500 °C and strain rate 0.1 s^{-1}.

Figure 6a shows that, for the aluminum alloy systems considered, the flow stress at 300 °C ranges from ~100 to ~200 MPa [35–39]. The highest values correspond to Al-Li alloys [35,36]. An increase in temperature up to 500 °C significantly reduces the above parameter, while reducing its range of variation to ~20 to 55 MPa. This is likely to make it impossible to operate products made from these materials under these conditions. However, AA2060 still appears preferable to alloys of other systems. A slightly different picture was obtained with aluminum alloy composites (see Figure 6b). The addition of 15 vol.% carbon fibers, as mentioned above, provides a flow stress value of 150 MPa at 300 °C, which is five times lower than the flow stress at a normal temperature [21]. This severe drop in strength properties is attributed by the authors to a weak interfacial interaction at elevated temperatures. This leads to a change in the composite fracture mechanism from fiber delamination to fracture at the interface. Approximately the same ~150 MPa value of flow stress was demonstrated by a composite based on the Al7075 alloy reinforced with 1.7 vol.% TiC particles of 50 nm average size [30]. A further increase in the test temperature to 400 °C led to a 2-fold decrease in flow stress to ~75 MPa. According to the authors, this was due to the slippage of the spherical nanoparticles with respect to the grain boundaries under load.

Paper [14] reported that the use of 1.5 wt.% Al_2O_3 particles with an average size of 20 nm to reinforce the alloy Al7075 provides softening reduction with increasing temperature. So, if at 300 °C, the flow stress was ~260 MPa, which is 13% lower than for A_CNT obtained in this work, then at 400 °C the difference does not exceed 5%. At 500 °C, the flow stress of the Al7075-based composite reinforced with 1.5 wt.% Al_2O_3 nanoparticles was already ~125 MPa, which is 30% higher than that of A_CNT. Data on the effect of SiC microparticle size on the heat resistance of Al7075 alloy are given in [37]. The authors show that increasing the average size of SiC microparticles from 5 to 63 μm at 15 vol.% reinforcement led to an increase in the flow stress of the composite material. For example, at 500 °C, the strain strength was 45 MPa and 140 MPa for 5 and 63 μm SiC-reinforced composites, respectively. The authors attribute this effect to the expansion of the Al–SiC interface and a change in the composite fracture mechanism from an adhesive one (along the matrix-reinforcing particle interface) to a transgranular one, in which cracks propagate through the reinforcing particles. The A_TiC/CNT composite material obtained in this work has approximately the same properties as the Al7075-alloy-based composite reinforced with 15 vol.% SiC with an average size of 63 μm. However, the reinforcement volume fraction in the case of A_TiC/CNT is ~23 times lower than that of the Al7075-based composite.

Thus, the presented results show that the surface modification of CNTs with nanoparticles, such as TiC, is a promising structure design strategy to increase the heat resistance of aluminum matrix composites.

4. Conclusions

Two types of bulk composites based on aluminum alloy reinforced with 1 wt.% of CNTs and 1 wt.% of TiC-coated CNTs were produced by powder metallurgy. Compression tests on these three bulk composites at 300–500 °C and a strain rate of 0.1 s^{-1} were performed. It was found that the composites obtained have 1.8–2.9 times higher flow stress at the above temperatures than a reference sample of matrix material without reinforcing particles, obtained by the same technological route. CNT-reinforced composites with TiC coating exhibited better properties than CNT-reinforced composites. For example, the presence of a TiC coating on the CNTs surface resulted in a 14–37% increase in the high-temperature flow stress at 300–500 °C compared with CNT-reinforced composites.

The results show that the use of TiC-coated CNTs as reinforcing particles expands the potential range of application of aluminum matrix composites as a structural material for operation at elevated temperatures. The surface modification of CNTs with ceramic nanoparticles is a promising structure design strategy to enhance the heat resistance of aluminum matrix composites.

Author Contributions: Conceptualization, A.V.A.; methodology, A.V.A.; formal analysis, D.V.B.; investigation, S.A.P.; data curation, D.V.B.; writing—original draft preparation, A.I.E.; writing—review and editing, A.V.A.; supervision, A.V.A.; funding acquisition, A.V.A. All authors have read and agreed to the published version of the manuscript.

Funding: This research was funded by the Russian Science Foundation (project No 18-79-10227).

Institutional Review Board Statement: Not applicable.

Informed Consent Statement: Not applicable.

Data Availability Statement: The data presented in this study are available in this article.

Acknowledgments: The study was carried out using the equipment of the interregional multispecialty and interdisciplinary center for the collective usage of promising and competitive technologies in the areas of development and application in industry/mechanical engineering of domestic achievements in the field of nanotechnology (Agreement No. 075-15-2021-692 of 5 August 2021).

Conflicts of Interest: The authors declare no conflict of interest.

References

1. Poletti, C.; Balog, M.; Simancik, F.; Degischer, H.P. High-temperature strength of compacted sub-micrometer aluminium powder. *Acta Mater.* **2010**, *58*, 3781–3789. [CrossRef]
2. Samal, P.; Vundavilli, P.R.; Meher, A.; Mahapatra, M.M. Recent progress in aluminum metal matrix composites: A review on processing, mechanical and wear properties. *J. Manuf. Process.* **2020**, *59*, 131–152. [CrossRef]
3. Deev, V.B.; Prusov, E.S.; Ri, E.H. Physical Methods of Processing the Melts of Metal Matrix Composites: Current State and Prospects. *Russ. J. Non-Ferr. Met.* **2022**, *63*, 292–304. [CrossRef]
4. Grilo, J.; Carneiro, V.H.; Teixeira, J.C.; Puga, H. Manufacturing Methodology on Casting-Based Aluminium Matrix Composites: Systematic Review. *Metals* **2021**, *11*, 436. [CrossRef]
5. Jendrzejewski, R.; Łubiński, J.; Śliwiński, G. Wear Resistance Enhancement of Al6061 Alloy Surface Layer by Laser Dispersed Carbide Powders. *Materials* **2020**, *13*, 3683. [CrossRef]
6. Li, K.; Liu, X.; Zhao, Y. Research Status and Prospect of Friction Stir Processing Technology. *Coatings* **2019**, *9*, 129. [CrossRef]
7. Jendrzejewski, R.; Van Acker, K.; Vanhoyweghen, D.; Śliwiński, G. Metal matrix composite production by means of laser dispersing of SiC and WC powder in Al alloy. *Appl. Surf. Sci.* **2009**, *255*, 5584–5587. [CrossRef]
8. Li, W.; Assadi, H.; Gaertner, F.; Yin, S. A review of advanced composite and nanostructured coatings by solid-state cold spraying process. *Crit. Rev. Solid State Mater. Sci.* **2019**, *44*, 109–156. [CrossRef]
9. Aborkin, A.V.; Alymov, M.I.; Arkhipov, V.E.; Khrenov, D.S. Formation of heterogeneous powder coatings with a two-level micro-and nanocomposite structure under gas-dynamic spraying conditions. *Dokl. Phys.* **2018**, *63*, 50–54. [CrossRef]
10. Moridi, A.; Hassani-Gangaraj, S.M.; Guagliano, M.; Dao, M. Cold Spray Coating: Review of Material Systems and Future Perspectives. *Surf. Eng.* **2014**, *36*, 369–395. [CrossRef]
11. Liu, J.; Huang, X.; Zhao, K.; Zhu, Z.; Zhu, X.; An, L. Effect of reinforcement particle size on quasistatic and dynamic mechanical properties of Al-Al_2O_3 composites. *J. Alloy. Compd.* **2019**, *797*, 1367–1371. [CrossRef]
12. Kang, Y.C.; Chan, S.L.I. Tensile properties of nanometric Al_2O_3 particulate-reinforced aluminum matrix composites. *Mater. Chem. Phys.* **2004**, *85*, 438–443. [CrossRef]
13. Prabhu, B.; Suryanarayana, C.; An, L.; Vaidyanathan, R. Synthesis and characterization of high volume fraction Al-Al_2O_3 nanocomposite powders by high-energy milling. *Mater. Sci. Eng. A* **2006**, *425*, 192–200. [CrossRef]
14. Saravanan, L.; Senthilvelan, T. Investigations on the hot workability characteristics and deformation mechanisms of aluminium alloy-Al2O3 nanocomposite. *Mater. Des.* **2015**, *79*, 6–14. [CrossRef]
15. Kashyap, K.T.; Patil, R.G. On Young's modulus of multi-walled carbon nanotubes. *Bull. Mater. Sci.* **2008**, *31*, 185–187. [CrossRef]
16. Wong, E.W.; Sheehan, P.E.; Lieber, C.M. Nanobeam mechanics: Elasticity, strength, and toughness of nanorods and nanotubes. *Science* **1997**, *277*, 1971–1975. [CrossRef]
17. Lourie, O.; Wagner, H.D. Evaluation of Young's modulus of carbon nanotubes by micro-Raman spectroscopy. *J. Mater. Res.* **1998**, *13*, 2418–2422. [CrossRef]
18. Yu, M.F.; Lourie, O.; Dyer, M.J.; Moloni, K.; Kelly, T.F.; Ruoff, R.S. Strength and breaking mechanism of multiwalled carbon nanotubes under tensile load. *Science* **2000**, *287*, 637–640. [CrossRef]
19. Peng, B.; Locascio, M.; Zapol, P.; Li, S.; Mielke, S.L.; Schatz, G.C.; Espinosa, H.D. Measurements of near-ultimate strength for multiwalled carbon nanotubes and irradiation-induced crosslinking improvements. *Nat. Nanotechnol.* **2008**, *3*, 626–631. [CrossRef]
20. Liu, Z.Y.; Xiao, B.L.; Wang, W.G.; Ma, Z.Y. Elevated temperature tensile properties and thermal expansion of CNT/2009Al composites. *Compos. Sci. Technol.* **2012**, *72*, 1826–1833. [CrossRef]
21. Lee, W.S.; Sue, W.C.; Lin, C.F. The effects of temperature and strain rate on the properties of carbon-fiber-reinforced 7075 aluminum alloy metal-matrix composite. *Compos. Sci. Technol.* **2000**, *60*, 1975–1983. [CrossRef]
22. Cao, L.; Chen, B.; Wan, J.; Kondoh, K.; Guo, B.; Shen, J.; Li, J.S. Superior high-temperature tensile properties of aluminum matrix composites reinforced with carbon nanotubes. *Carbon* **2022**, *191*, 403–414. [CrossRef]
23. Aborkin, A.V.; Khor'kov, K.S.; Ob'edkov, A.M.; Kremlev, K.V.; Izobello, A.Y.; Volochko, A.T.; Alymov, M.I. Evolution of Multiwalled Carbon Nanotubes and Related Nanostructures during the Formation of Alumomatrix Composite Materials. *Tech. Phys. Lett.* **2019**, *45*, 20–23. [CrossRef]
24. Aborkin, A.V.; Babin, D.M.; Zalesnov, A.I.; Prusov, E.S.; Ob'edkov, A.M.; Alymov, M.I. Effect of ceramic coating on carbon nanotubes interaction with matrix material and mechanical properties of aluminum matrix nanocomposite. *Ceram. Int.* **2020**, *46*, 19256–19263. [CrossRef]
25. Aborkin, A.V.; Khorkov, K.S.; Prusov, E.S.; Ob'edkov, A.M.; Kremlev, K.V.; Perezhogin, I.A.; Alymov, M.I. Effect of Increasing the Strength of Aluminum Matrix Nanocomposites Reinforced with Microadditions of Multiwalled Carbon Nanotubes Coated with TiC Nanoparticles. *Nanomaterials* **2019**, *9*, 1596. [CrossRef] [PubMed]
26. Kremlev, K.V.; Ob'edkov, A.M.; Semenov, N.M.; Kaverin, B.S.; Ketkov, S.Y.; Vilkov, I.V.; Andreev, P.V.; Gusev, S.A.; Aborkin, A.V. Synthesis of Hybrid Materials Based on Multiwalled Carbon Nanotubes Decorated with WC_{1-x} Nanocoatings of Various Morphologies. *Tech. Phys. Lett.* **2019**, *45*, 348–351. [CrossRef]
27. Aborkin, A.V.; Elkin, A.I.; Reshetniak, V.V.; Ob'edkov, A.M.; Sytschev, A.E.; Leontiev, V.G.; Titov, D.D.; Alymov, M.I. Thermal expansion of aluminum matrix composites reinforced by carbon nanotubes with in-situ and ex-situ designed interfaces ceramics layers. *J. Alloy. Compd.* **2021**, *872*, 159593. [CrossRef]

28. Guo, B.; Luo, S.; Wu, Y.; Song, M.; Chen, B.; Yu, Z.; Li, W. Regulating the interfacial reaction between carbon nanotubes and aluminum via copper nano decoration. *Mater. Sci. Eng. A* **2021**, *821*, 141576. [CrossRef]
29. Contreras, A. Wetting of TiC by Al-Cu alloys and interfacial characterization. *J. Colloid Interface Sci.* **2007**, *311*, 159–170. [CrossRef]
30. Huang, C.C.; Qi, L.; Chen, J.; Guan, R.; Ojo, O.A.; Wang, Z.G. Effect of TiC nanoparticles on the hot deformation behavior of AA7075 aluminum alloy. *Mater. Charact.* **2021**, *181*, 111508. [CrossRef]
31. Jagannatham, M.; Chandran, P.; Sankaran, S.; Haridoss, P.; Nayan, N.; Bakshi, S.R. Tensile properties of carbon nanotubes reinforced aluminum matrix composites: A review. *Carbon* **2020**, *160*, 14–44. [CrossRef]
32. Obiedkov, A.M.; Kaverin, B.S.; Egorov, V.A.; Semenov, N.M.; Ketkov, S.Y.; Domrachev, G.A.; Kremlev, K.V.; Gusev, S.A.; Perevezentsev, V.N.; Moskvichev, A.N.; et al. Macroscopic cylinders on the basis of radial-oriented multiwall carbon nanotubes. *Lett. Mater.* **2012**, *3*, 152–156. [CrossRef]
33. Vilkov, I.V.; Kaverin, B.S.; Ob'edkov, A.M.; Semenov, N.M.; Ketkov, S.Y.; Rychagova, E.A.; Gusev, S.A.; Tatarskiy, D.A.; Andreev, P.V.; Aborkin, A.V. Single-step synthesis of tic mesocrystals on the mwcnts surface by the pyrolysis of Cp_2TiCl_2. *Mater. Today Chem.* **2022**, *24*, 100830. [CrossRef]
34. Aborkin, A.V.; Alymov, M.I.; Sobol'kov, A.V.; Khor'kov, K.S.; Babin, D.M. Effect of the Thermomechanical Treatment Conditions on the Consolidation, the Structure, and the Mechanical Properties of Bulk Al–Mg–C Nanocomposites. *Russ. Metall.* **2018**, *2018*, 625–632. [CrossRef]
35. Ou, L.; Zheng, Z.; Nie, Y.; Jian, H. Hot deformation behavior of 2060 alloy. *J. Alloys Compd.* **2015**, *648*, 681–689. [CrossRef]
36. Avramovic-Cingara, G.; McQueen, H.J.; Perovic, D.D. Comparison of torsion and compression constitutive analyses for elevated temperature deformation of Al–Li–Cu–Mn alloy. *Mater. Sci. Technol.* **2014**, *19*, 11–19. [CrossRef]
37. Rajamuthamilselvan, M.; Rajakumar, S.; Kavitha, S. Effect of Different SiCp Particle Sizes on the Behavior of AA 7075 Hot Deformation Composites Using Processing Maps. *Springer Proc. Mater.* **2021**, *5*, 1233–1244.
38. Lin, H.B. Dynamic recrystallization behavior of 6082 aluminum alloy during hot deformation. *Adv. Mech. Eng.* **2021**, *13*, 11. [CrossRef]
39. Ding, S.; Khan, S.A.; Yanagimoto, J. Constitutive descriptions and microstructure evolution of extruded A5083 aluminum alloy during hot compression. *Mater. Sci. Eng. A* **2018**, *728*, 133–143. [CrossRef]